9

Supplementary Materials

Understanding and Attributing Climate Change

Coordinating Lead Authors:

Gabriele C. Hegerl (USA, Germany), Francis W. Zwiers (Canada)

Lead Authors:

Pascale Braconnot (France), Nathan P. Gillett (UK), Yong Luo (China), Jose A. Marengo Orsini (Brazil, Peru), Neville Nicholls (Australia), Joyce E. Penner (USA), Peter A. Stott (UK)

Contributing Authors:

M. Allen (UK), C. Ammann (USA), N. Andronova (USA), R.A. Betts (UK), A. Clement (USA), W.D. Collins (USA), S. Crooks (UK), T.L. Delworth (USA), C. Forest (USA), P. Forster (UK), H. Goosse (Belgium), J.M. Gregory (UK), D. Harvey (Canada), G.S. Jones (UK), F. Joos (Switzerland), J. Kenyon (USA), J. Kettleborough (UK), V. Kharin (Canada), R. Knutti (Switzerland), F.H. Lambert (UK), M. Lavine (USA), T.C.K. Lee (Canada), D. Levinson (USA), V. Masson-Delmotte (France), T. Nozawa (Japan), B. Otto-Bliesner (USA), D. Pierce (USA), S. Power (Australia), D. Rind (USA), L. Rotstayn (Australia), B. D. Santer (USA), C. Senior (UK), D. Sexton (UK), S. Stark (UK), D.A. Stone (UK), S. Tett (UK), P. Thorne (UK), R. van Dorland (The Netherlands), M. Wang (USA), B. Wielicki (USA), T. Wong (USA), L. Xu (USA, China), X. Zhang (Canada), E. Zorita (Germany, Spain)

Review Editors:

David J. Karoly (USA, Australia), Laban Ogallo (Kenya), Serge Planton (France)

Chapter 9 Supplementary Material

Appendix 9.B: Methods Used to Estimate Climate Sensitivity and Aerosol Forcing

Recent studies estimating climate sensitivity from observations can all be cast in terms of an approach that is closely related to climate change detection methods.

In this approach, observed climate change T_{obs} (x.t) , where x and t indicate space and time coordinates, is repeatedly compared to each of a series of climate change simulations T (x, t, θ) obtained from a climate model by varying the elements of a small vector θ of model parameters. A relatively simple climate model is typically used in this approach because of the large number of simulations that are required and because such models often explicitly include parameters such as the equilibrium climate sensitivity. The parameters that are varied from one climate simulation to the next typically include the equilibrium climate sensitivity α and other important determinants of the climate response to greenhouse gas forcing. The latter may include the effective vertical diffusivity of the ocean κ (which controls the rate at which heat anomalies penetrate into the deep ocean) or a parameter representing a range of possible aerosol forcings ε_{aer}.

Depending on the study, the comparison between observations and model is performed either only in time (i.e., after integrating T (x, t, θ) and T_{obs} (x.t) over the space coordinate x) or in both space and time. Also, depending on the study, T and T_{obs} can represent either a scalar variable such as surface temperature, or a vector composed of several variables such as surface temperature, upper-air temperature, top-of-atmosphere or surface fluxes and/or and deep-ocean temperature.

A variety of statistics have been used to evaluate the agreement between model and observations for a given set of parameters, θ. Knutti et al. (2002) assess the probability of globally averaged temperatures being consistent with observations by calculating the probability of the observed change given the model simulation, its uncertainty and observational uncertainty. Forest et al. (2001; 2002) first calculate the residual mean square r^2(θ, T_{obs}) = $(T(θ)–T_{obs})^T$ C^{-1} $(T(θ)–T_{obs})$ where C^{-1} is the inverse covariance matrix of internal climate variability estimated from control simulations with AOGCMs. As in optimal detection methods, this statistic measures residual variability after transforming the model response and observations so that the former is optimally detectable in the latter (Allen and Tett, 1999; see Appendix 9.A).The same square residual, but without the inverse covariance weighting, was used by Hegerl et al. (2006). The residual mean square is subsequently used to evaluate the likelihood of the given parameter choice. For example, assuming that noise is Gaussian, the likelihood can be evaluated by using the fact that the relative difference between any residual and the minimum residual, $\Delta r^2/(r^2_{min})$, will be distributed according to the F-distribution with m and ν degrees of freedom (Forest et al., 2002; 2006) where m is the number of free parameters in the model simulation, and ν is the number of degrees of freedom of the residual climate variability.

In either case, the end result is a likelihood function $p(T_{obs}|θ)$ that describes how the likelihood of the observations changes as the parameters θ vary. This function, together with a prior distribution on the parameters, can be combined by means of Bayes theorem to obtain a posterior distribution $p(θ|T_{obs})$ on the parameters. That is, one calculates $p(θ|T_{obs}) \propto p(T_{obs}|θ) p(θ)$ where the product on the right is normalized so that the integral of $p(θ|T_{obs})$ with respect to θ is equal to one. Finally, if one is interested in making inferences only about one of the parameters contained in θ, say the climate sensitivity, the posterior density function $p(θ|T_{obs})$ is integrated over the ranges of other elements of θ to obtain the marginal posterior probability density function for the parameter of interest.

An important consideration is the representation of the expected discrepancy between observed and simulated temperatures due to, for example, observational uncertainty, forcing uncertainty or internal climate variability. These uncertainties affect the width of the likelihood function, and thus the width of the posterior distribution. Properties of internal climate variability "noise" must be estimated from either models or residual variability. Care is required because underestimates of noise will result in narrow posterior distributions that do not adequately portray the real uncertainty of parameters of interest.

The prior distribution p(θ) that is used in this calculation is chosen to reflect prior knowledge and uncertainty (either subjective or objective) about plausible parameter values, and in fact, is often simply a wide uniform distribution. Such a prior indicates that little is known, a priori, about the parameters of interest except that they are bounded below and above. Even so, the choice of prior bounds can be subjective. In the case of climate sensitivity, a uniform prior with a lower bound of 0°C and an upper bound between 10°C and 20°C has often been used (see Table 9.3). However, observable properties of the climate system do not necessarily scale with equilibrium climate sensitivity (Frame et al., 2005). Imposing a flat prior on an observable property, such as the climate feedback or transient climate response, is equivalent to imposing a highly skewed prior on the equilibrium climate sensitivity, and therefore results in narrower posterior likelihood ranges on the climate sensitivity that exclude very high sensitivities. Alternatively, expert opinion can also be used to construct priors (Forest et al., 2002; 2006). Note, however, that expert opinion may be overconfident (Risbey and Kandlikar, 2002) and if this is the case, the posterior distribution may be too narrow. Also, the information used to derive the expert prior needs to be independent from the information that is used to estimate the likelihood function. However, prior belief about the climate system tends to be shaped by observations of that system, and thus it is difficult, maybe even impossible, to develop truly independent prior distributions.

Appendix 9.C: Notes and Technical Details on Figures Displayed in Chapter 9

Figure 9.1

Figure 9.1 shows zonally-averaged temperature changes as a function of latitude (90°N-90°S) and height (from 1000 hPa to 10 hPa). Temperature changes are expressed as linear trends in degrees Celsius per century, and were calculated over the period from 1890 to 1999. All results are ensemble means (averages over four individual realizations).

Figure 9.2

Figure 9.2 is based on the difference between preindustrial and present day in 2 simulations run to steady state.

Figure 9.3

The models plotted in Figure 9.3 were those available with all the requisite data in June 2005 (when the analysis was performed). The model data were only available as monthly averages, while ERBS data were only available as 72-day averages. Therefore,

72-day averages were estimated for the models by interpolating the monthly data from the models. A check was performed to determine whether this procedure would create any biases in the trends and anomalies by comparing anomalies from true 72-day averages from ISCCP FD 3-hourly data and from monthly averaged ISCCP FD data. There were no significant seasonal differences or any trend from using this procedure. The outgoing shortwave flux anomaly for each model and data set was calculated relative to the 15 year average from 1985 through 1999.

Linear trends (in Wm^{-2}/yr for the 15 year time period) were fitted to the data and the 95% confidence interval for the difference in the trend from the ERBS data and all other data sets are found in the following table.

Figure 9.5

This figure was plotted from annual mean anomalies computed following steps 1, 2, 4, 5, and 7-10 for FAQ 9.2, Figure 1 (that is, steps 1-10 without land or ocean masking).

Comparison of Outgoing SW TOA Trend table (60ºS-60ºN)

	Name	Trend (W m^{-2}/year)	95% confidence level	Difference trend (model-ERBS) (W m^{-2}/year)	95% confidence level for difference
Satellite	ERBS	-0.1267	0.079	/	/
ISCCP	monthly	-0.1798	0.1129	-0.0375	0.0849
	3hrly	-0.1796	0.1133	-0.0368	0.0842
Model	cccma_cgcm3_1_t47	-0.0224	0.0187	0.1025	0.0885
	cccma_cgcm3_1_t63	-0.0382	0.0158	0.0862	0.084
	cnrm_cm3	-0.0101	0.038	0.1179	0.0944
	csiro_mk3_0	0.0076	0.011	0.134	0.0778
	gfdl_cm2_0	-0.0273	0.0595	0.1208	0.0439
	gfdl_cm2_1	-0.015	0.0577	0.1276	0.0474
	giss_aom	-0.0011	0.0116	0.1221	0.082
	giss_model_e_h	-0.0173	0.0777	0.1391	0.0474
	giss_model_e_r	-0.0237	0.0729	0.1282	0.044
	iap_fgoals1_0_g	0.0247	0.0157	0.153	0.082
	inmcm3_0	0.0299	0.04	0.1744	0.061
	ipsl_cm4	-0.0396	0.0163	0.0836	0.0823
	mri_cgcm2_3_2a	-0.0788	0.0558	0.0618	0.0536
	ncar_ccsm3_0	-0.0245	0.0486	0.1186	0.0461
	miroc3_2_hires	0.0098	0.0372	0.1389	0.0561
	miroc3_2_medres	-0.012	0.0304	0.1158	0.0596
	miub_echo_g	-0.0184	0.0635	0.1231	0.042
	ncar_pcm1	0.0019	0.0726	0.1531	0.0493
	ukmo_hadcm3	0.0027	0.1371	0.1349	0.158
	ukmo_hadgem1	-0.0309	0.033	0.1117	0.058

Figure 9.6

This figure was plotted using annual means from Step 1-8 of the data processing procedure described for FAQ 9.2, Figure 1, which were then further processed by re-centering relative to 1901-1997 (left panels) and 1979-1997 (right panels). Grid points with missing annual means for a period of 6 consecutive years or longer are excluded. Red and blue shading in the bottom panels indicate the "middle" 90% of simulated trends determined as in step 12 of the procedure for FAQ 9.2, Figure 1.

Figure 9.7

Data processing for this figure was performed as for Figure 9.6. The power spectra were estimated using the method described in Mitchell et al. (2001), Figure 12.2.

Figure 9.8

This figure was produced identically to Figure 9.7, except continental means were used. See description of FAQ 9.2, Figure 1, for a description of regions.

Figure 9.12

This figure was produced identically to FAQ 9.2, Figure 1, except the sub-continental regions listed in the description of that figure are used.

Figure 9.16

The observed DJF mean sea level pressure trends shown are based on the infilled dataset HadSLP2r over 1955-2005 (Allan and Ansell, 2006). A grid point trend from the infilled dataset is marked as missing if no grid points within 550 km have more than 50% of observed monthly anomalies present in all five decadal means. The same mask was applied to the model-based trends. If the detection study of Gillett et al. (2005) is repeated using the infilled HadSLP2r data presented here, results similar to those published are obtained, and external forcing remains detectable.

FAQ 9.2, Figure 1

Detailed caption:

Continental, global, global land, and global ocean decadal mean temperature anomalies relative to the period 1901-1950. The black lines show observed temperature anomalies from HadCRUT3 (Brohan et al., 2006). Dashed black lines indicate decades and continental regions for which the fractional spatial coverage is less than 50%.

The red bands represent approximate ranges covering the middle 90% of 58 simulations of the climate of the 20th century with prescribed anthropogenic and natural forcings from 14 climate models that did not exhibit excessive drift in their control simulations (no more than 0.2°C per century). The blue bands were determined similarly using 19 simulations with prescribed natural forcings only from 5 models. The model data were masked with the pattern of observed missing data and were subsequently processed identically to the observations.

Model simulations including both anthropogenic and natural forcings are: CCSM3 (8 simulations), ECHO-G (5), GFDL-CM2.0 (3), GFDL-CM2.1 (5), GISS-EH (5), GISS-ER (9), INM-CM3.0 (1), MIROC3.2(medres) (4), MRI-CGCM2.3.2 (5), PCM (4), UKMO-HadCM3 (4), UKMO-HadGEM1 (1). Details for these models are provided in Table 8.1. Two additional models included in the data are ECHAM4-OPYC3 (1 simulation) and GFDL-R30 (3).

Model simulations including natural forcings only are: ECHO-G (3 simulations), MIROC3.2(medres) (4), MRI-CGCM2.3.2 (4), PCM (4), UKMO-HadCM3 (4). Model details are provided in Table 8. 1.

Detailed description of the procedures used to produce this figure:

1. Quality control
To ensure adequate data in the climatological base period of 1961-1990, observed data for each calendar month at a grid cell were retained only if 50% or more of monthly values over the 1961-1990 period exist for that calendar month and grid cell. See Note 1 for a list of observational datasets used.

2. Select simulations
An ensemble of 58 "ALL" forcing simulations (i.e., with historical anthropogenic and natural forcings) was formed from 14 models. Simulations ending before 2005 were extended to 2005 by using the first few years of the SRES A1B scenario simulations that continued from the respective ALL simulations, where available. An ensemble of 19 "NAT" forcing simulations (i.e., with historical natural forcings only) was formed from 5 models. See Note 1 below for the list of simulations. Models from the multi-model data archive at PDMDI (MMD) were included in these ensembles if they had a control run that drifted only modestly (i.e., less than 0.2K/century drift in global mean temperature).

3. Apply land or ocean mask on simulations
Plots describing simulated changes in land or ocean areas were based on model output that was masked to retain land or ocean data only. For a given model, data in a grid cell were retained for land or ocean plots if the land area fraction (indicated by the variable sftlf in the MMD data archive) was greater than or equal to 0.5 (land) or less than 0.5 (ocean) for that grid cell.

4. Interpolate model output to a standard grid
The masked model output (from Step 3) was interpolated onto the 5°x5° grid of the observed data (from Step 1). A weighted-area-overlap interpolation scheme was used. That is, a weighted mean of the cells that overlap the cell in the observed data grid was calculated, where the weighting was determined by the area of overlap.

5. Apply observational mask
Data in a given month and grid cell in the simulation data sets (from Step 4) were retained only if there was a corresponding value in that month and grid cell in the observed data set (from Step 1).

6. Apply land/ocean mask on observations
Plots describing observed changes in land or ocean areas were based on observed data that was masked to retain land or ocean data only (necessary to remove islands and marine stations not existent in models). This masking was performed as in Step 3, using the land area fraction data from the CCSM3 model.

7. Deseasonalise all data
For all data sets (both simulations from Step 5 and observations from Step 6), anomalies were calculated for each month and grid cell relative to the 1961-1990 base period average from the respective calendar month for that grid cell.

8. Calculate annual averages
For all data sets from Step 7, an annual average was calculated at each grid cell for each year in which at least 6 monthly anomalies were available at that grid cell.

9. Calculate spatial averages
For all data sets from Step 8, a weighted spatial average was calculated for a given region for each year. The weighting was determined by the area of overlap between grid cells and the region's borders as calculated from the CCSM3 land mask (from Step 6). Note that this and all subsequent steps were repeated for each region considered. See Note 2 for a list of regions.

10. Calculate anomalies relative to the 1901-1950 reference period
For all of the data sets from Step 9, time series were re-centered relative to the mean of the 1901-1950 reference period for that time series.

11. Calculate decadal averages
For all data sets from Step 10, an average was calculated for each decade in the period 1906-2005, beginning with the decade of 1906-1915, if at least one annual average was available for the given decade. The maximum fractional spatial coverage for each decade (i.e., the maximum of the weights determined in Step 9) was recorded for each decade.

12. Determine the range of spread between simulations
For the ALL simulations, for each decade, each of the decadal averages from Step 11 were ranked in increasing order. The

values of the two simulations closest to the edges of the middle 90% of simulations for that decade (i.e. the 4th and 55th of the 58 sorted ALL simulations) were retained to indicate the range of decadal averages spanned by as close to 90% of simulations as possible. A similar approximate 90% range was determined from NAT simulations as the 2nd and 18th of the 19 sorted NAT simulations.

13. Plot results
The approximate 90% ranges from Step 12 were displayed for both the ALL ensemble (in red) and the NAT ensemble (in blue). The observation time series from Step 11 was plotted as a solid black line when the fractional spatial coverage (also from Step 11) is greater than or equal to 50% and as a dashed black line otherwise.

14. Repeat for all regions
Steps 9 to 13 for all regions listed in Note 2.

15. Calculate and plot linear trends
Linear trends over the period beginning in 1951 were calculated for time series of annual averages from Step 10 for selected regions, using the same colour convention as in Step 13. These supplementary plots are displayed in Appendix 9.D, Figure S9.1.

Note 1: Lists of Simulations and Obervations

List of Simulations

Notes and headings:

• 20C3M ALL: historical simulation with both natural and anthropogenic forcings

• 20C3M NAT: historical simulation with natural forcings only

• SRES A1B: 20C3M ALL simulation extended using years from a consecutive simulation following the SRES A1B scenario

• Each row represents a single 20C3M ALL simulation.

• 20C3M NAT simulations are listed on the same row as the corresponding 20C3M ALL simulations (i.e. the one with the same initial state).

• The period covered under each scenario is given in the corresponding column.

• For model details see: Appendix 9.D; Supplementary material, Table S9.1; Table 8.1; and McAvaney et al. (2001), Table 8.1.

MODEL	20C3M ALL (SRES A1B)		20C3M NAT	
ECHAM4-OPYC3	1	1901-2000		
GFDL-CM2.0	2	1901-2000 (2001-2005)		
	3	1901-2000		
	4	1901-2000		
GFDL-CM2.1	5	1901-2000		
	6	1901-2000 (2001-2005)		
	7	1901-2000		
	8	1901-2000		
	9	1901-2000		
GFDL-R30	10	1901-1998		
	11	1901-1998		
	12	1901-1998		
GISS-EH	13	1901-1999 (2000-2005)		
	14	1901-1999 (2000-2005)		
	15	1901-1999 (2000-2005)		
	16	1901-1999		
	17	1901-1999		
GISS-ER	18	1901-2003		
	19	1901-2003		
	20	1901-2003 (2004-2005)		
	21	1901-1999		
	22	1901-1999		
	23	1901-2003 (2004-2005)		
	24	1901-2003 (2004-2005)		
	25	1901-2003 (2004-2005)		
	26	1901-2003 (2004-2005)		
INM-CM3.0	27	1901-2000 (2001-2005)		
MIROC3.2(medres)	28	1901-2000 (2001-2005)	1	1901-2001
	29	1901-2000 (2001-2005)	2	1901-2001
	30	1901-2000 (2001-2005)	3	1901-2001
	31	1901-2000	4	1901-2001
ECHO-G	32	1901-2000 (2001-2005)	5	1901-2000
	33	1901-2000 (2001-2005)	6	1901-2000
	34	1901-2000 (2001-2005)	7	1901-2000
	35	1901-2000		
	36	1901-2000		

MRI-CGCM2.3.2	37	1901-2000 (2001-2005)	8	1901-1999
	38	1901-2000 (2001-2005)	9	1901-1999
	39	1901-2000 (2001-2005)	10	1901-1999
	40	1901-2000 (2001-2005)	11	1901-1999
	41	1901-2000 (2001-2005)		
CCSM3	42	1901-1999 (2000-2005)		
	43	1901-1999 (2000-2005)		
	44	1901-1999 (2000-2005)		
	45	1901-1999		
	46	1901-1999 (2000-2005)		
	47	1901-1999 (2000-2005)		
	48	1901-1999 (2000-2005)		
	49	1901-1999		
PCM	50	1901-1999	12	1901-1999
	51	1901-1999	13	1901-1999
	52	1901-1999	14	1901-1999
	53	1901-1999	15	1901-1999
UKMO-HadCM3	54	1901-2005	16	1901-1999
	55	1901-2002	17	1901-1999
	56	1901-2002	18	1901-1999
	57	1901-2002	19	1901-1999
UKMO-HadGEM1	58	1901-1999		

List of Observations

OBSERVATION DATASET	COVERAGE	PERIOD	REFERENCE
HadCRUT3	land+ocean	1901-2005	Brohan et al. (2006)
CRUTEM3	land	1901-2005	Brohan et al. (2006)
HadSST2	ocean	1901-2005	Rayner et al. (2006)

Note 2: List of Regions

The regions are defined as the collection of rectangular boxes listed for each region. The domain of interest (land and ocean, land, or ocean) is also given. Definitions for the regions in each continent are from Giorgi and Francisco (2000a,b).

REGION	DESIGNATOR	COVERAGE	DOMAIN
Global	GLO	180W to 180E, 90S to 90N	land and ocean
Global Land	LAN	180W to 180E, 90S to 90N	land
Global Ocean	OCE	180W to 180E, 90S to 90N	ocean
North America	ALA	170W to 103W, 60N to 72N	land
	CGI	103W to 10W, 50N to 85N	land
	WNA	130W to 103W, 30N to 60N	land
	CNA	103W to 85W, 30N to 50N	land
	ENA	85W to 50W, 25N to 50N	land
South America	CAM	116W to 83W, 10N to 30N	land
	AMZ	82W to 34W, 20S to 12N	land
	SSA	76W to 40W, 56S to 20S	land
Europe	NEU	10W to 40E, 48N to 75N	land
	SEU	10W to 40E, 30N to 48N	land
Africa	SAR	20W to 65E, 18N to 30N	land
	WAF	20W to 22E, 12S to 18N	land
	EAF	22E to 52E, 12S to 18N	land
	SAF	10E to 52E, 35S to 12S	land
Asia	NAS	40E to 180E, 50N to 70N	land
	CAS	40E to 75E, 30N to 50N	land
	TIB	75E to 100E, 30N to 50N	land
	EAS	100E to 145E, 20N to 50N	land
	SAS	65E to 100E, 5N to 30N	land
	SEA	95E to 155E, 11S to 20N	land
Australia	NAU	110E to 155E, 30S to 11S	land
	SAU	110E to 155E, 45S to 30S	land

Appendix 9D:
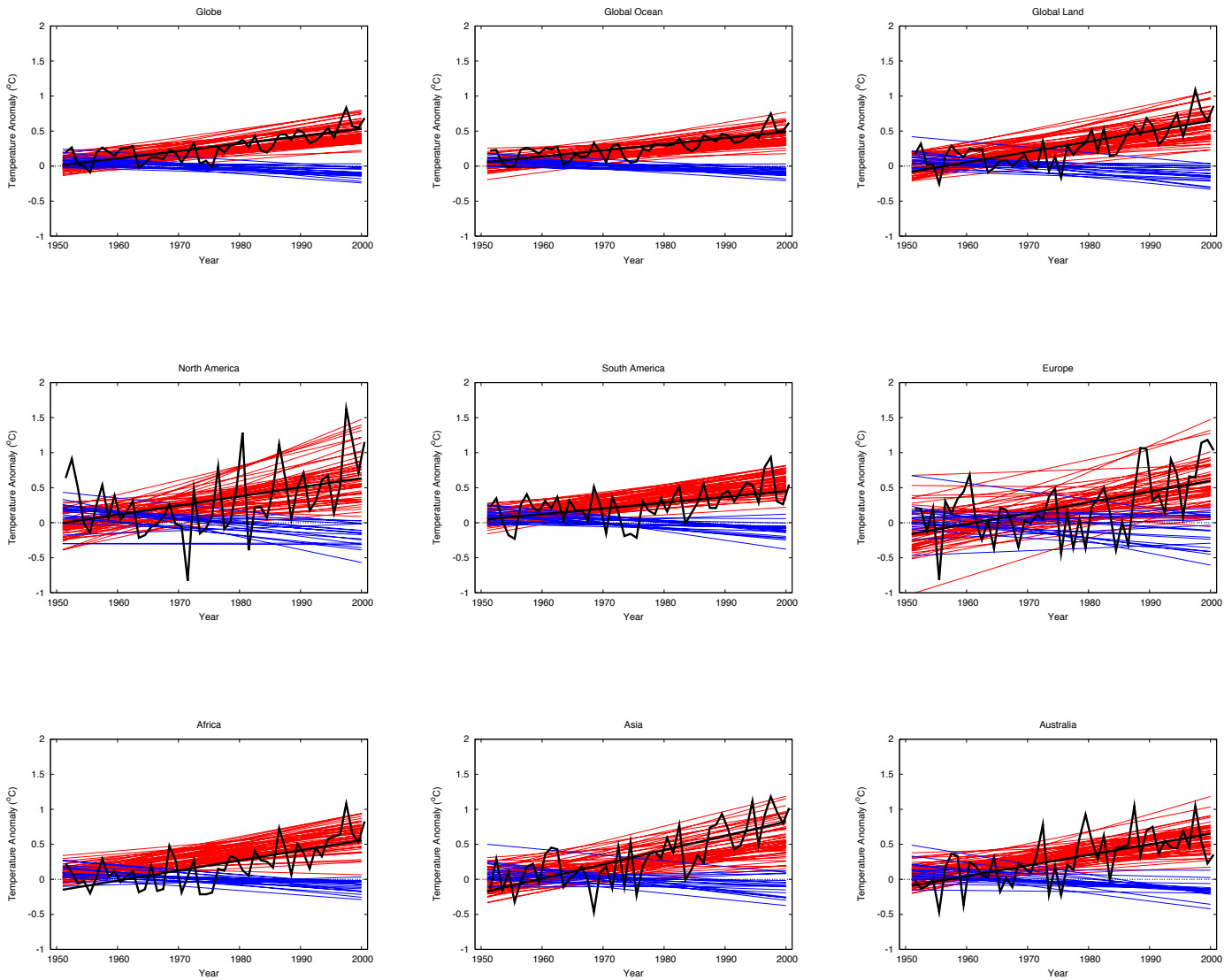# Additional Figures and Tables

Figure S9.1: *Linear trends in area mean surface temperature anomalies for the period 1951-2000 for observations (black), 58 "ALL" simulations from 14 models using historical anthropogenic and natural forcing (red) and 19 "NAT" simulations from 5 models using historial natural forcing only. Observed annual mean anomalies relative to 1901-1950 are also shown. Data and regions are as for FAQ 9.2, Figure 1. Data were processed following Steps 1-10 of the procedure for FAQ 9.2, Figure 1. No model that has used natural forcing only has reproduced the observed global mean warming trend or the continental mean warming trends in all individual continents (except Antarctica where there is insufficient data to perform an analysis) over the second half of the 20th century.*

Table S9.1. Models used in chapter 9 to evaluate simulations of 20th century climate change with both anthropogenic and natural forcings and with natural forcings only.

AOGCM	A+N ?	N ?	GHG	DSU	ISU	VOL	SOL	BCA	TOZ	SOZ	LAN	Ref
1: BCC-CM1, China	N	N										
2: BCCR-BCM2.0, Norway	N	N										
3: CCSM3, USA	N	N	y	y	y	Amm	L95	M	Moz2	K99		Meehl et al. (2006)
4: CGCM3.1(T47), Canada	N	N										
5: CGCM3.1(T63), Canada	N	N										
6: CNRM-CM3, France	N	N										
7: CSIRO-Mk3.0, Australia	N	N										
8: ECHAM5/MPI-OM, Germany	N	N										
9: ECHO-G, Germany/Korea	5	3	y	y	y	C00	L95 (C00)					Min and Hense (2006)
10: FGOALS-g1.0, China	N	N										
11: GFDL-CM2.0, USA	5	N	y	y		RS	L95	C	Moz1	RW	HU	Knutson et al. (2006)
12: GFDL-CM2.1, USA	3	N	y	y	y	RS	L95	C	Moz1	RW	HU	As above
13: GISS-AOM, USA	N	N										
14: GISS-EH, USA	5	N	y	y	y	S93	L02	HA	SHI	RW1	RF	Hansen et al. (2005), Schmidt et al. (2006)
15: GISS-ER, USA	9	N	y	y	y	S93	L02	HA	SHI	RW1	RF	As GISS-EH
16: INM-CM3.0, Russia	1	N	y	y		Amm	HS					Diansky and Volodin (2002)
17: IPSL-CM4, France	N	N										
18: MIROC3.2(hires), Japan	N	N										
19: MIROC3.2(medres), Japan	4	4	y	y		S93	L95	NOZ	SUD	RW	HI	Nozawa et al, (2005)
20: MRI-CGCM2.3.2, Japan	5	4	y	y		S93	L95					
21: PCM, USA	4	4	y	y		Amm	HS		K99	K99		Meehl et al. (2004)
22: UKMO-HadCM3, UK	4	4	y	y	y	S93	L95		STO	RW		Tett et al. (2002)
23: UKMO-HadGEM1, UK	1	N	y	y	y	S93	SK	NOZ	STO	RW	G01	Stott et al. (2006)
ECHAM4 OPYC3	1	N	y	y	y	R01/ Amm	L95				G01	Stendel et al. (2006)
GFDL R30	3	N	y	y	y	A99	L00					Broccoli et al. (2003)

The 2nd and 3rd columns of the Table show, for each of the AOGCMs listed in Table 8.1 and for two additional AOGCMs, whether climate simulations from these models have been included in the analysis shown in Figure 9.5, Figure 9.12 and FAQ 9.2, Figure 1, and if so, how many simulations have been included with both anthropogenic and natural forcings (column "A+N ?") and how many simulations have been included with just natural forcings (column "N?"). Where simulations with that combination of forcings of that AOGCM have not been included, "N" is shown in the relevant column. The 4th to 12th columns show whether particular forcings were included in that model (indicated by "y"), where the key below describes the forcing. For GHG, DSU, ISU, the reader is referred to the paper detailed in the final column of the paper for further details and to details given at http://www-pcmdi.llnl.gov/ipcc/model_documentation.php.

For VOL, SOL, BCA, TOZ, SOZ, LAN, the forcing used in that model is listed by an abbreviation in the table where the key below lists the relevant forcing and appropriate reference.

Key

GHG = greenhouse gases
See ref in column 13 and http://www-pcmdi.llnl.gov/ipcc/model_documentation.php for further details.

DSU = direct effect of tropospheric sulfates
See ref in column 13 and http://www-pcmdi.llnl.gov/ipcc/model_documentation.php for further details.

ISU = indirect effect of tropospheric sulfates
See ref in column 13 and http://www-pcmdi.llnl.gov/ipcc/model_documentation.php for further details.

VOL = volcanic (stratospheric) aerosols
A99: Andronova et al. (1999).
Amm: Ammann et al. (2003).
C00: temporally varying solar constant (Crowley, 2000)
Rob 01/Amm: Robertson et al. (2001) to 1889, and Ammann et al. (2003) from 1890.
RS: Ramachandran et al. (2000). Pinatubo estimates altered slightly and blended with Sato et al. (1993) estimates, then Sato et al. (1993) values used for eruptions going back to 1860.
S93: Sato et al. (1993). Updated. See Hansen et al. (2005).

SOL = solar irradiance
L95: Lean et al. (1995).
L95 (C00): temporally varying solar constant based on Lean et al. (1995) (Crowley, 2000).
L00: Lean (2000).
L02: Lean et al. (2002).
HS: Hoyt and Schatten (1993).
SK: Solanki and Krivova (2003).

BCA = black carbon
C: Cooke et al. (1999).
HA: Hansen et al. (2005).
M : Meehl et al. (2006).
NOZ : Carbonaceous aerosols are provided by T. Nozawa (unpublished data, 2005), a brief description of which is given by Takemura et al. (2005) and more detailed description is available at http://atm-phys.nies.go.jp/~nozawa/emission.

TOZ = tropospheric ozone
K99: A synthesis of observed and where observed data are absent model-generated data (Kiehl et al., 1999).
Moz1: MOZART chemistry-transport model-generated distributions (Horowitz et al., 2003; Tie et al., 2005); "1990" climatology from NCAR's MACCM3 used for all years; emission values used are estimates at the beginning of each decade.
Moz2: MOZART chemistry-transport model-generated distributions (Horowitz et al., 2003; Tie et al., 2005); snapshot runs every 20 years : 1890, 1910, 1930, 1950, 1970, 1990 on T42 18L resolution with meteorology from PCM all forcings 20th century run (Meehl et al., 2004).
SHI : A chemical transport model was run for the period 1850-2000 driven by prescribed changes in ozone precursor emissions and climate conditions. This provides an estimate for the effect of tropospheric air pollution on tropospheric O3 (Shindell et al., 2003).
SUD: Tropospheric ozone estimated by the chemical model of Sudo et al. (2002).
STO: Three-dimensional fields of monthly-mean tropospheric ozone were computed using the off-line STOCHEM chemistry transport model (Collins et al., 1997).

SOZ = stratospheric ozone
K: Kiehl et al. (1999).
RW: Randel and Wu (1999).
RW1: Randel and Wu (1999). There was an error in the implementation of the Randel and Wu trend in stratospheric ozone in the GISS-EH and GISS-ER simulations. This led to an underestimate of the changes from 1979 to 1997 by a factor of 5/9. Updated runs using a correct ozone trend will be forthcoming, but preliminary tests indicate that only the lower stratospheric temperature trends are much affected. Surface radiative forcing is very similar (leading to about 0.01°C difference in the 120 year change, which is less than the run to run variability).

LAN = land use
G01: Goldewijk (2001).
HI : Hirabayashi et al. (2005).
HU : Hurtt et al. (2006) global land use reconstruction history, including effect on surface albedo, surface roughness, stomatal resistance, and effective water capacity.
RF: Ramankutty and Foley (1999).

References

Allen, M.R., and S.F.B. Tett, 1999: Checking for model consistency in optimal fingerprinting. Climate Dynamics, 15, 419-434.

Allan, R.J., and T.J. Ansell, 2006: A new globally complete monthly historical mean sea level pressure data set (HadSLP2): 1850-2004. Journal of Climate, accepted.

Ammann, C.M., G.A. Meehl, W.M. Washington, and C. Zender, 2003: A monthly and latitudinally varying volcanic forcing dataset in simulations of 20th century climate. Geophysical Research Letters, 30(12), 1657.

Andronova, N.G., E.V. Rozanov, F. Yang, M.E. Schlesinger, and G.L. Stenchikov, 1999: Radiative forcing by volcanic aerosols from 1850 to 1994. Journal of Geophysical Research, 104, 16,807-16,826.

Broccoli, A.J., et al., 2003: Twentieth-century temperature and precipitation trends in ensemble climate simulations including natural and anthropogenic forcing. Journal of Geophysical Research, 108(D24), 4798.

Brohan, P., J.J. Kennedy, I. Haris, S.F.B. Tett, and P.D. Jones, 2006: Uncertainty estimates in regional and global observed temperature changes: a new dataset from 1850. Journal of Geophysical Research, 111(D12106).

Collins, W., D. Stevenson, and C. Johnson, 1997: Tropospheric ozone in a global-scale three-dimensional Lagrangian model and its response to NOx emission. Journal of Atmospheric Chemistry, 26, 223-274.

Cooke, W.F., C. Liousse, H. Cashier, and J. Feichter, 1999: Construction of a 1 x 1 fossil fuel emission dataset for carbonaceuous aerosol and implementation and radiative impact in the ECHAM-4 model. Journal of Geophysical Research, 104, 22137-22162.

Crowley, T.J., 2000: Causes of climate change over the past 1000 years. Science, 289(5477), 270-277.

Diansky, N.A., and E.M. Volodin, 2002: Simulation of present-day climate with a coupled Atmosphere-ocean general circulation model. Izvestia, Atmospheric and Oceanic Physics, 38, 732-747.

Forest, C.E., M.R. Allen, A.P. Sokolov, and P.H. Stone, 2001: Constraining Climate Model Properties Using Optimal Fingerprint Detection Methods. Climate Dynamics, 18, 277-295.

Forest, C.E., P.H. Stone, A.P. Sokolov, M.R. Allen, and M.D. Webster, 2002: Quantifying uncertainties in climate system properties with the use of recent observations. Science, 295, 113.

Forest, D.J., P.H. Stone, and A.P. Sokolov, 2006: Estimated PDFs of climate system properties including natural and anthropogenic forcings. Geophysical Research Letters, 33, L01705.

Frame, D.J., et al., 2005: Constraining climate forecasts: The role of prior assumptions. Geophysical Research Letters, 32, L09702.

Gillett, N.P., R.J. Allan, and T.J. Ansell, 2005: Detection of external influence on sea level pressure with a multi-model ensemble. Geophysical Research Letters, 32(19), L19714.

Giorgi, F. and R. Francisco, 2000a; Evaluating uncertainties in the prediction of regional climate. Geophysical Research Letters, 27, 1295-1298.

Giorgi, F. and R. Francisco, 2000b: Uncertainties in regional climate change prediction: a regional analysis of ensemble simulations with the HadCM2 coupled AOGCM. Climate Dyn., 16, 169-182.

Goldewijk, K.K., 2001: Estimating global land use change over the past 300 years: The HYDE Database. Global Biogeochemical Cycles, 15(2), 417-433.

Hansen, J., et al., 2005: Efficacy of climate forcings. Journal of Geophysical Research, 110, D18104.

Hegerl, G.C., T. Crowley, W.T. Hyde, and D. Frame, 2006: Constraints on climate sensitivity from temperature reconstructions of the past seven centuries. Nature, 440, doi:10.1038/nature04679.

Hirabayashi, Y., S. Kanae, I. Struthers, and T. Oki, 2005: A 100-year (1901-2000) global retrospective estimation of the terrestrial water cycle. Journal of Geophysical Research, 108, 4784.

Horowitz, L.W., et al., 2003: A global simulation of tropospheric ozone and related tracers: description and evaluation of MOZART, version 2. Journal of Geophysical Research, 108, 4784.

Hoyt, D.V., and K.H. Schatten, 1993: A discussion of plausible solar irradiance variations, 1700-1992. Journal of Geophysical Research, 98, 18895-18906.

Hurtt, G.C., et al., 2006: The underpinnings of land-use history: three centuries of global gridded land-use transitions, wood-harvest activity, and resulting secondary lands. Global Change Biology, 12, 1208-1229.

Kiehl, J.T., T.L. Schneider, R.W. Portmann, and S. Solomon, 1999: Climate forcing due to tropospheric and stratospheric ozone. Journal of Geophysical Research, 104(D24), 31239-31254.

Knutson, T.R., et al., 2006: Assessment of twentieth-century regional surface temperature trends using the GFDL CM2 coupled models. Journal of Climate, 19, 1624-1651.

Knutti, R., T.F. Stocker, F. Joos, and G.-K. Plattner, 2002: Constraints on radiative forcing and future climate change from observations and climate model ensembles. Nature, 416, 719-723.

Lean, J., 2000: Evolution of the sun's spectral irradiance since the Maunder Minimum. Geophysical Research Letters, 27(16), 2425-2428.

Lean, J.L., J. Beer, and R. Bradley, 1995: Reconstruction of solar irradiance changes since 1610: Implications for climate change. Geophysical Reserach Letters, 22, 3195.

Lean, J.L., Y.M. Wang, and N.R. Sheeley, 2002: The effect of increasing solar activity on the Sun's total and open magnetic flux during multiple cycles: Implications for solar forcing of climate. Geophysical Research Letters, 29(24), 2224, doi:10.1029/2002GL015880.

McAvaney, B.J., et al., 2001: Model Evaluation. In: IPCC, 2001: Climate Change 2001: The Scientific Basis. Contribution of Working Group I to the Third Assessment Report of the Intergovernmental Panel on Climate Change [J.T. Houghton, et al. (eds.)]. Cambridge University Press, New York, pp. 471-525.

Meehl, G.A., et al., 2004: Combinations of natural and anthropogenic forcings in 20th century climate. Journal of Climate, 17, 3721-3727.

Meehl, G.A., et al., 2006: Climate change projections for the twenty-first century and climate change commitment in the CCSM3. J. Clim., 19, 2597-2616.

Min, S.-K., and A. Hense, 2006: A Bayesian assessment of climate change using multi-model ensembles. Part I: Global mean surface temperature. Journal of Climate, 19, 3237-3256.

Mitchell, J.F.B., D.J. Karoly, G.C. Hegerl, F.W. Zwiers, and J. Marengo, 2001: Detection of climate change and attribution of causes. In: Climate Change 2001. The Scientific Basis. The Contribution of Working Group I to the Third Assessment Report of the Intergovernmental Panel on Climate Change. [J.T. Houghton, et al. (eds.)]. Cambridge University Press, New York, NY, USA, pp. 695-738.

Nozawa, T., T. Nagashima, H. Shiogama, and S. Crooks, 2005: Detecting natural influence on surface air temperature in the early twentieth century. Geophysical Research Letters, 32, L20719.

Ramachandran, S., V. Ramaswamy, G.L. Stenchikov, and A. Robock, 2000: Radioactive impact of the Mt. Pinatubo volcanic eruption: Lower stratospheric response. Journal of Geophysical Research, 105, 24409-24429.

Ramankutty, N., and J.A. Foley, 1999: Estimating historical changes in global land cover: Croplands from 1700 to 1992. Global Biogeochemical Cycles, 13(4), 997-1027.

Randel, W.J., and F. Wu, 1999: A stratospheric ozone trends data set for global modeling studies. Geophysical Research Letters, 26, 3089-3092.

Rayner, N.A., et al., 2006: Improved analyses of changes and uncertainties in marine temperature measured in situ since the mid-nineteenth century: the HadSST2 dataset. Journal of Climate, 19(446-469).

Risbey, J.S., and M. Kandlikar, 2002: Expert Assessment of Uncertainties in Detection and Attribution of Climate. Bulletin of the American Meteorological Society, 83, 1317–1326.

Robertson, A., et al., 2001: Hypothesized climate forcing time series for the last 500 years. Journal of Geophysical Research-Atmospheres, 106(D14), 14783-14803.

Sato, M., J.E. Hansen, M.P. McCormik, and J.B. Pollack, 1993: Stratospheric aerosol optical depths, 1850-1990. Journal of Geophysical Research, 98, 22987-22994.

Schmidt, G.A., et al., 2006: Present-Day Atmospheric Simulations Using GISS ModelE: Comparison to In Situ, Satellite, and Reanalysis Data. Journal of Climate, 19, 153-192.

Shindell, D., G. Fulavegi, and N. Bell, 2003: Preindustrial-to-present-day radiative forcing by tropospheric ozone from improved simulations with the GISS chemistry-climate GCM. Atmospheric Chemistry and Physics, 3, 1675-1702.

Solanki, S., and N. Krivova, 2003: Can solar variability explain global warming since 1970? Journal of Geophysical Research, 108, 1200.

Stendel, M., I.A. Mogensen, and J.H. Christensen, 2006: Influence of various forcings on global climate in historical times using a coupled atmosphere–ocean general circulation model. Climate Dynamics, 26, 1-15.

Stott, P.A., et al., 2006: Transient climate simulations with the HadGEM1 model: causes of past warming and future climate change. J. Clim., 19, 2763-2782.

Sudo, K., M. Takahashi, J. Kurokawa, and H. Akamito, 2002: CHASER: A global chemical model of the troposphere 1. Model description. Journal of Geophysical Research, 107(D17), 4339.

Takemura, T., T. Nozawa, S. Emori, T.Y. Nakajima, and T. Nakajima, 2005: Simulation of climate response to aerosol direct and indirect effects with aerosol transport-radiation model. Journal of Geophysical Research, 110, D02202.

Tett, S.F.B., et al., 2002: Estimation of natural and anthropogenic contributions to twentieth century temperature change. Journal of Geophysical Research, 107(D16), 4306, doi:10.1029/2000JD000028.

Tie, X., et al., 2005: Assessment of the global impact of aerosols on tropospheric oxidants. Journal of Geophysical Research, 110, D03204.